AN UPDATE ABOUT FLUKA

A. Fassò*, A.Ferrari#, J. Ranft†, P.R.Sala#
* CERN, 1211 Geneva 23, Switzerland
# INFN sez. di Milano, via Celoria 16, I-20133 Milano, Italy
† LAPP, Chemin de Bellevue, BP 110, F-74941 Annecy-le-vieux Cedex, France.

Abstract

The most recent improvements to the physical models of the FLUKA code are described. They concern mainly the transport of charged particles (scattering and ionization) and the hadron generators at intermediate and high energies. The increased accuracy and predictive power of FLUKA are shown by examples, which allow to consider new fields of application for the code.

1 INTRODUCTION

The FLUKA history and the program structure have been described in several publications and conferences during the last four years [1, 2, 3, 4, 5, 6, 7, 8, 9]. Development of the code is still in continuous progress, concerning both the user interface and the physical models. In this contribution only the most recent improvements to the latter are described.

The condensed-history algorithm used for charged particle scattering, complemented by the possibility of resorting to single scattering at boundary crossing (or on user request), is now free from an artefact present in most transport codes. The treatment of ionization in compound materials has been refined leading to a better representation of the distribution of energy deposited by heavy charged particles near the end of their range.

However, the most important achievements regard the intermediate energy model for hadron interactions, where the inclusion of a variety of new effects (neutron halo, quantal effects, Fermi break-up of light nuclei, anisotropy of particle emission following pion absorption, isobar model description of pion production) has lead to better predictions about residual nuclei, double differential yields and fission cross sections. The high energy model has also been improved.

2 CHARGED PARTICLE TRANSPORT

2.1 Improvements in the multiple Coulomb scattering

The model used in FLUKA for multiple Coulomb scattering is based on the Molière theory, and to our knowledge is the only one which takes into account correlations between path length corrections and scattering angle, and also between the lateral deflection and the scattering angle [1].

However, the Molière algorithm for multiple scattering has its intrinsic limits of validity: it can be applied only if the path length is long enough to allow that at least a few

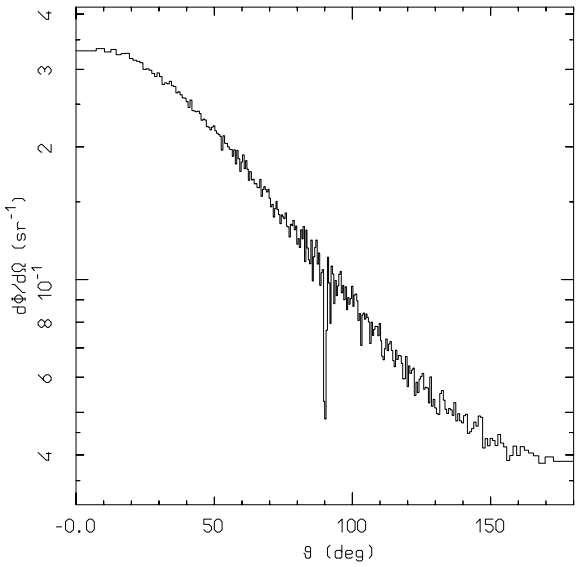

Figure 1: Angular distribution of 1 MeV electrons traversing a fictitious plane boundary in a homogeneous Al slab, obtained with the complete single scattering algorithm.

(>20–30) elementary scatterings are performed, and short enough to limit the average deflection angle below one radian. The first condition can fail in the case of very thin layers, or wires, or gaseous materials, or even in approaching a boundary between two different materials, while the two conditions become incompatible in heavy materials at low energies.

Single scattering To cope with all these situations, a single scattering algorithm has been developed for FLUKA. The form for the single scattering cross section has been taken again from the Molière derivations [10, 11], in order to be consistent with the existing multiple scattering algorithm. It can be written as:

$$\frac{d\sigma_M}{d\Omega} = \frac{d\sigma_R}{d\Omega} \cdot \left[\frac{(1-\cos\theta)^2}{\left(1-\cos\theta+\frac{1}{2}\chi_a^2\right)^2} \right] \quad (1)$$

where $\frac{d\sigma_R}{d\Omega}$ is the Rutherford cross section, and the term in square brackets comes from atomic screening. The χ_a parameter is the Molière screening angle. Equation 1 can be integrated analytically without approximations, and the resulting function can be directly sampled from. Moreover, additional corrections (nuclear, spin-relativistic) can be applied in a straightforward way with a simple rejection

method.

The single scattering algorithm can be used standalone therefore switching off the multiple scattering model, but of course the CPU penalty is quite large (from 50 to 100 times), or it can be used in conjunction with the multiple scattering model as described in the following paragraphs.

The boundary artefact A problem arising in simulating electron transport with condensed history Monte Carlo codes has been pinpointed in a recent paper [12]. The authors called it the "boundary artefact", as it shows up in an unphysical peak at 90° in the fluence angular distribution on boundaries, even in the case of a fictitious boundary inserted in an homogeneous region, and reflects itself also in the energy deposition distribution. In [12] the artefact was discovered using EGS4/PRESTA and it was ascribed to the lack of correlations between path length corrections and scattering angle, and inconsistencies in the lateral correlation algorithm. While these deficiencies are present in the PRESTA algorithm, it turns out, however, that such boundary artefact is a more general problem, due to the forced truncation of steps on boundaries for whichever condensed history Monte Carlo code, regardless of the specific model used.

Suppose to have an electron beam travelling along the z axis in an infinite homogeneous medium, and to simulate a plane boundary at $z = \bar{z}$. In a perfect calculation this boundary should have no effect on any physical quantity, and this is indeed what happens if one uses a single scattering algorithm to perform the charged particle transport, as shown in fig. 1 (the values around 90° suffer from poor statistics due to the grazing incidence and to the large amount of CPU required by the single scattering algorithm). When using a condensed history Monte Carlo, many scatterings are lumped in a single step on the basis of material dependent quantities. Steps that would cross a boundary between different materials must therefore be shortened and forced somehow to end on the boundary itself, and the same happens even on a fictitious boundary. Since the angular deflection is then applied at the end of the step, the boundary becomes an area of accumulation of scattering centres. In particular, particles crossing the boundary at $\approx 90^\circ$ can be only those scattered the last time in the close proximity of the boundary itself. It is qualitatively clear that the physical finite value of the fluence for $\theta \to 90^\circ$ comes from the product of the "weighting" factor $1/\cos\theta$ for each particle crossing the boundary times the number of scattering events occurring in a neighborhood of the surface, which becomes narrower and narrower for $\theta \to 90^\circ$. If the density of scattering events remains finite and possibly continuous also close to the boundary no problem occurs, but for condensed history models there is always a finite number of scatterings occurring just *on* the surface and therefore in a sufficiently small neighborhood the density can become as large as one wants.

A quantitative proof is given in the following, for the case of normal incidence. We consider the case of a parallel beam of particles travelling in the z direction, and encountering a plane boundary perpendicular to the z axis at $z = 0$. Let us call λ the mean free path between scatterings, $P(\theta)$ the probability density of scattering at an angle θ, and $\rho(z)$ the linear density of particles undergoing a scattering at a position z. To calculate the fluence of particles crossing the boundary at an angle θ, and coming from the last collision event, one has to add the contributions of all the particles scattered at any z in the direction θ, weighted by the probability of reaching the boundary before being rescattered and by the geometrical factor $1/\cos\theta$ coming from the definition of fluence. As the distance between the scattering point and the boundary is given by $\frac{|z|}{\cos\theta}$, one has:

$$\frac{d\Phi}{d\Omega} = \int_{-\infty}^{0} \rho dz \frac{P(\theta)}{\cos\theta} \mathrm{e}^{-\frac{|z|}{\lambda \cos\theta}} \tag{2}$$

If the density of scatterings $\rho(z)$ is that of single scatterings, it has again an exponential form:

$$\rho(z) = \rho_0 \mathrm{e}^{-\frac{|z|}{\lambda}} \tag{3}$$

and the integral in Eq. 2 gives

$$\frac{d\Phi}{d\Omega} = \frac{\lambda \rho_0}{1 + \cos\theta} P(\theta) \tag{4}$$

that is a smooth function of the angle θ. A similar expression would be obtained in the case of Molière multiple scatterings steps without truncations, which gives a $\rho(z)$ without singularities. If, conversely, the scatterings are concentrated on the boundary due to step truncation, the density takes the form of a δ distribution, and the fluence becomes (ρ_M is the normalization factor)

$$\frac{d\Phi}{d\Omega} = \lambda \frac{\rho_M}{\cos\theta} P(\theta) \tag{5}$$

with an evident discontinuity at $\theta = 90^\circ$.

The "One Step Back" Algorithm The proposed solution is the inclusion of one (or more) single scattering steps at the boundary crossing ("one step back" correction). In doing this we exploit the fact that a Molière step is nothing more than the convolution of many single scattering steps. In practice, when a multiple scattering step is truncated on a boundary, a single step path length is sampled and its length is randomly divided in two fractions, one before the boundary and one after it. The fraction before the boundary is used to calculate the ideal position of the last scattering centre in the multiple scattering step, and the Molière deflection is applied at this point. From this point the particle is transported along its new direction for the previously sampled single scattering path length, and then the multiple scattering transport starts again. At the user's choice, the procedure can involve more than one single scattering step.

The effectiveness of this algorithm is shown in figs. 2, 3 where the artefact and its elimination are shown. In these, as in the previous one, the statistics of the single scattering calculation is still low, due to the huge amount of CPU time per event. In all these plots the multiple scattering steps

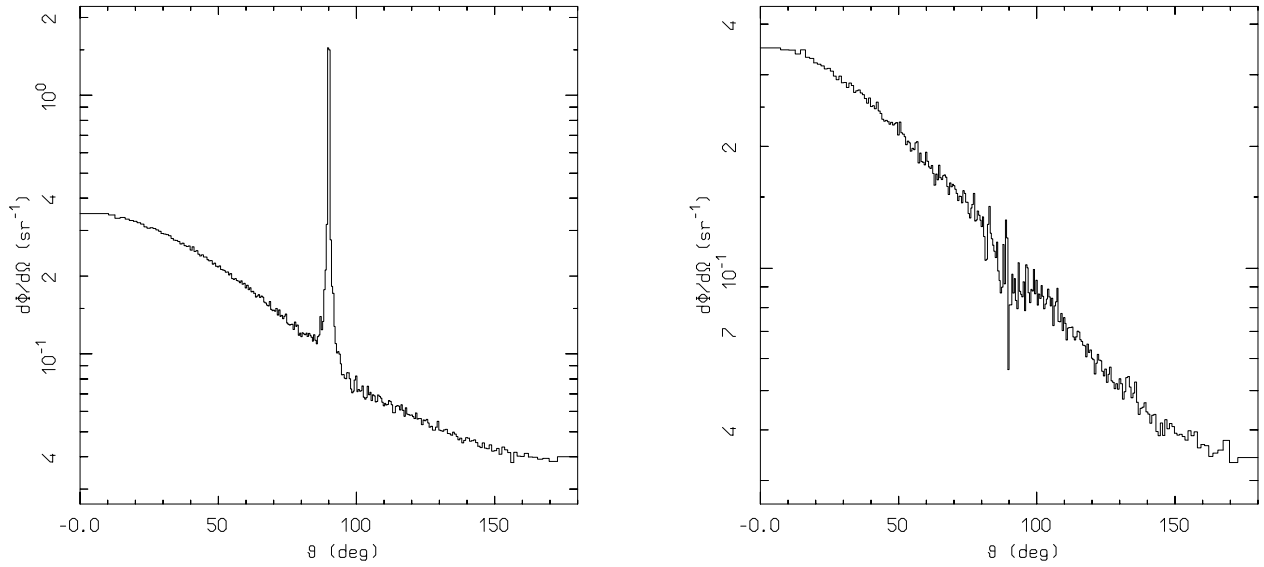

Figure 2: Angular distribution of 1 MeV electrons traversing a fictitious plane boundary in an homogeneous Al slab, obtained with the complete multiple scattering algorithm (left) and with the "one step back" correction (right).

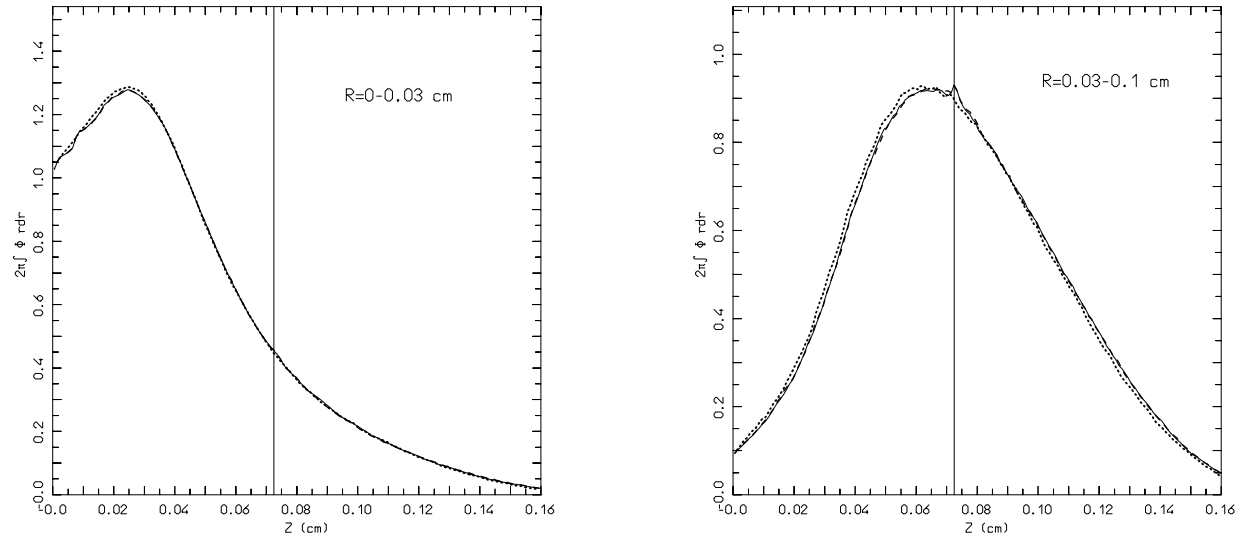

Figure 3: Radially integrated fluence due to a pencil beam of 1 MeV electron as a function of the depth in an homogeneous Al slab. The position of a fictitious plane boundary is shown by the vertical line. Results integrated over two different radial ranges are shown. Full lines are obtained with the multiple scattering algorithm with "one step back" correction, dashed lines are multiple scattering, dotted lines are completely single scattering.

were quite long, being fixed to give a 10% energy loss per step. Nonetheless, the agreement between single and multiple scattering is good, except for a small difference in fluence at large radii. This difference does not depend on step length, neither on the correction algorithm, and seems to be inherent in the Molière formulation.

The advantages of a hybrid solution From this story a few remarks on the generality of boundary crossings in condensed history codes arise naturally.

The problem of boundary crossing is not treated in any multiple scattering theory. The solution to this discontinuity has to be found in an empirical way, and can lead to biases and distortions like the one described above. For instance, long steps in proximity of a boundary can lead to an underestimation of the boundary crossing probability, and to an enhanced probability to travel along the boundary, since the simulated straight path fails to reproduce a physical wiggly path repeatedly crossing the boundary. This is solved in FLUKA with a smooth approach to boundaries, obtained by progressively shortening the path length as the charged particle approaches the discontinuity. The addition of the "one step back" correction is a further refinement of

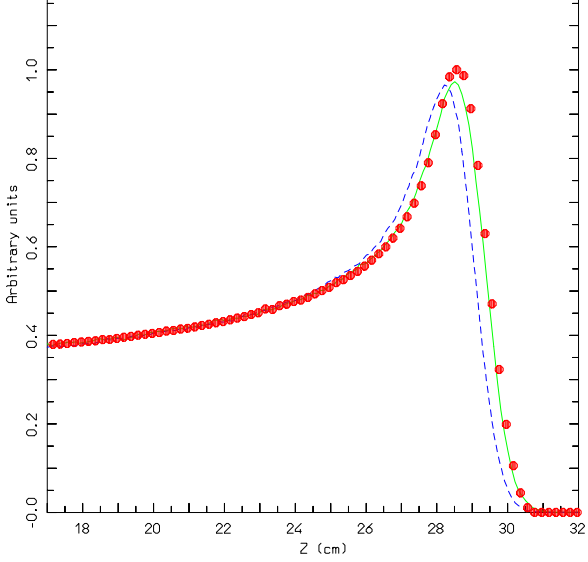

Figure 4: Energy deposition in water due to a 214 MeV proton beam, as obtained with a ionization potential given by Bragg's rule (dashed line) and with the recommended value for water (dotted line), compared with experimental data [16] (symbols).

this smooth approach. Moreover, the joining of a multiple scattering algorithm with a single scattering one can be very useful in problems involving edge scattering, or heavy materials, or backscattering. A last reminder: all charged particles, not only electrons are transported using the multiple scattering algorithm, thus all the considerations made here apply as well to protons, muons, pions...

2.2 Ionization

To evaluate the unrestricted energy loss of heavy charged particles in elemental substances, FLUKA makes use of the Bethe-Bloch formula with ionization potential and density effect parameters taken from the compilation of Sternheimer, Seltzer and Berger [13].

Shell corrections are derived from a parametrized formula for unrestricted dE/dx obtained by Ziegler and Andersen [14] fitting available experimental proton data up to 100 MeV. Shell corrections and average ionization potential values do not appear explicitly in the formula, but can be deduced by comparison with the Bethe-Bloch expression in order to ensure a consistent approach when delta rays are generated on user's request and the corresponding restricted energy loss is needed.

In the case of compounds and mixtures, the Bragg additivity formula is used by default. The remark is often made that, although deviations from stopping power additivity have been reported, the effect on calculated energy deposition is small due to the logarithmic dependence of dE/dx on average ionization potential. However, there are cases where not only *the amount* of energy deposition is important, but one must also accurately determine *where* it is deposited. A good example is given by hadron therapy, where it is essential to know with great accuracy the position of the Bragg peak with respect to that of the tumour to be treated. It can be seen in fig. 4 that using a best estimated value of ionization potential can substantially improve the agreement between the calculated and the measured position of the Bragg peak. Therefore the possibility is now offered to the user to override on request both the default ionization potential and the density effect parameters for compounds. It is thus possible to benefit from good compilations such as those of Sternheimer, Seltzer and Berger [13], whenever the relevant parameters of the compound under investigation are known. Anyway the suggestions given in the report [15] to improve the average ionization potential of liquid and solid compounds over the naive Bragg additivity rule are applied whenever the material under consideration is not included in the available compilations.

Other additions to the treatment of energy loss are the possibility to define materials with local density different from average (porous substances), and the ranging out of particles below transport cutoff. The latter is done in an approximate way (although taking into account boundaries and magnetic fields), but improves the quality of calculated dose distributions, avoiding for instance known artefacts such as accumulation of high dose "spots" on boundaries.

3 INTERMEDIATE ENERGY HADRONIC INTERACTIONS

The model used in FLUKA (called PEANUT) for hadronic energies in the range 0-1.5 GeV has already been described elsewhere [4, 6, 7, 9]. It combines both an intranuclear cascade (INC) part, and a preequilibrium part, with a smooth transition around 50 MeV for secondary nucleons, and 30 MeV for primary ones. Nuclear potential effects (refraction and reflection) are modeled into the code, as well as quantal effects, like Pauli blocking, nucleon-nucleon correlations, fermion antisymmetrization, coherence length and formation zone.

In the following, we will present the most recent developments of the model, but before this, it is interesting to show how the various stages and effects included in PEANUT contribute to overcome most of the weaknesses of old plain INC treatments, like the glorious Bertini [17, 18] model.

It is important to remind that the Bertini model does not include reflection or refraction, neither includes any preequilibrium stage. Furthermore an average binding energy is used throughout all cascading process without account for actual Q values of the different reaction channels.

In order to illustrate the effect of the various ingredients, the same projectile-target combination, 80.5 MeV protons on ^{90}Zr, has been computed under different assumptions and the results compared with experimental data [19, 20]. Four different trials have been performed, always using PEANUT with all or only a few of the ingredients at work. The results of the exercise are presented in figs. 5,6,7,8, for (p,xn), and in figs. 9,10,11,12, for (p,xp). In all these figures, as well as in following ones, experimental data are plotted as full symbols joined by a line, while model re-

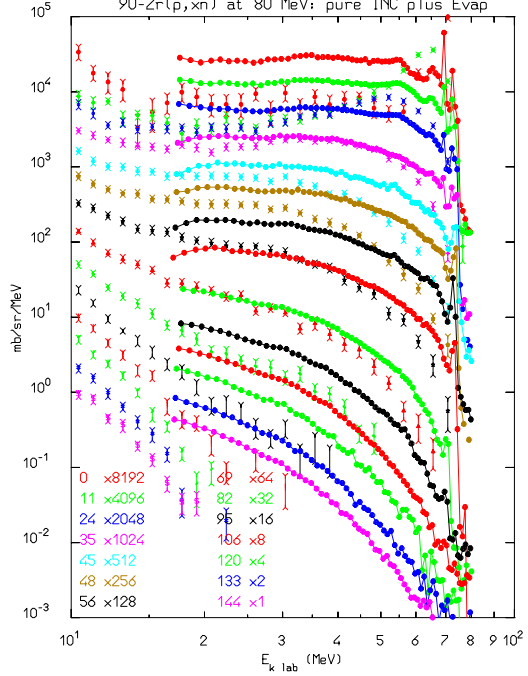

Figure 5: ^{90}Zr(p,xn) at 80.5 MeV, plain INC (see text) calculation.

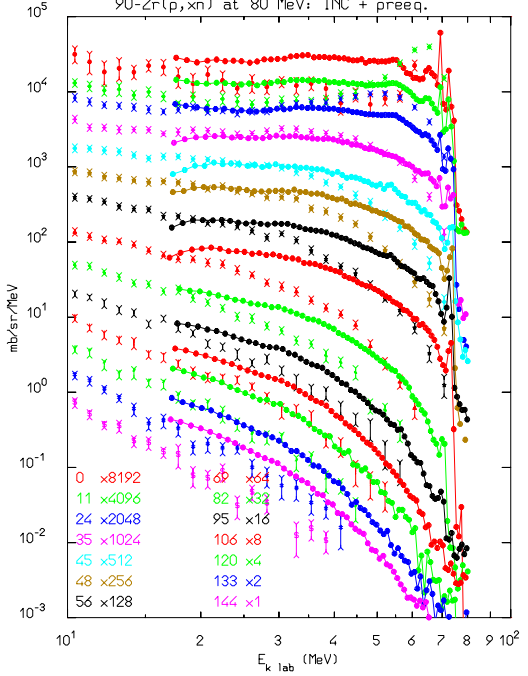

Figure 6: ^{90}Zr(p,xn) at 80.5 MeV, plain INC plus preequilibrium (see text) calculation.

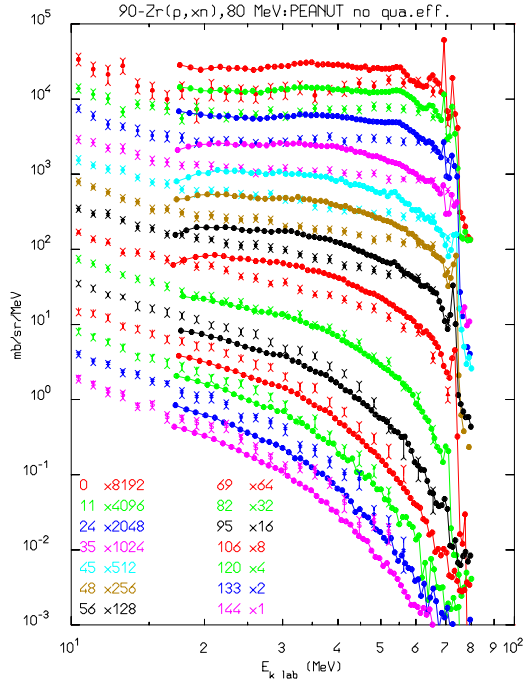

Figure 7: ^{90}Zr(p,xn) at 80.5 MeV, PEANUT (see text) calculation with no quantal effect, but Pauli blocking.

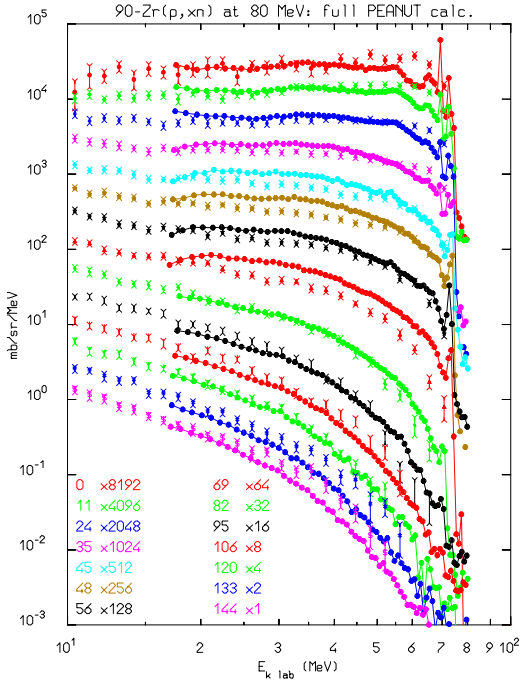

Figure 8: ^{90}Zr(p,xn) at 80.5 MeV, full PEANUT (see text) calculation.

sults are given either by symbols with error bars, or by histograms with shaded areas representing the statistical error.

The first attempt (figs. 5,9) has been performed using a plain INC approach with no preequilibrium stage, no refraction and reflection, and only Pauli blocking activated among the quantal effects. The transport threshold for secondary nucleons was set equal to the average binding energy. The binding energy has been correctly set at each emission stage to match the actual reaction Q-value. As can be easily seen results are very poor, with an overestimation of the forward peak and a strong underestimation of backward angle emission. Other codes using a similar INC treatment give similar results, as can be seen for instance in [21].

The second trial does not yet use refraction and reflection, but the preequilibrium stage is there. There is a clear improvement in the results, particularly at backward angles,

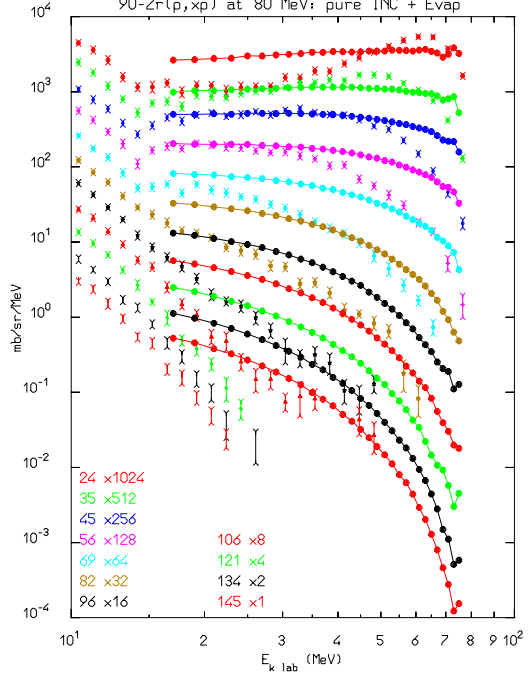

Figure 9: ^{90}Zr(p,xp) at 80.5 MeV, plain INC (see text) calculation.

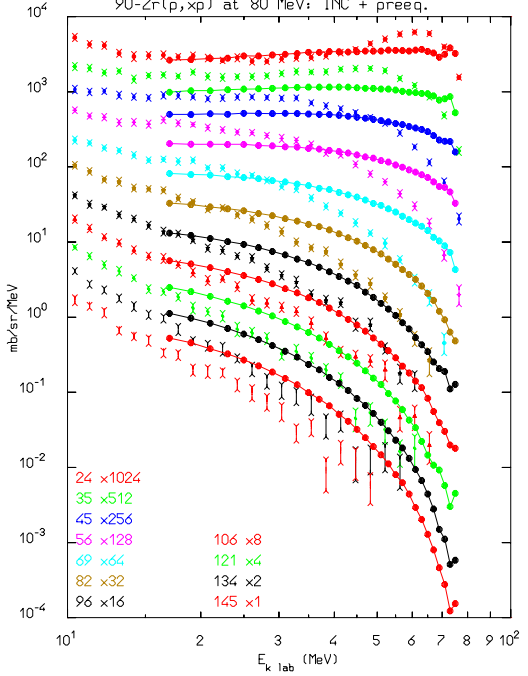

Figure 10: ^{90}Zr(p,xp) at 80.5 MeV, plain INC plus preequilibrium (see text) calculation.

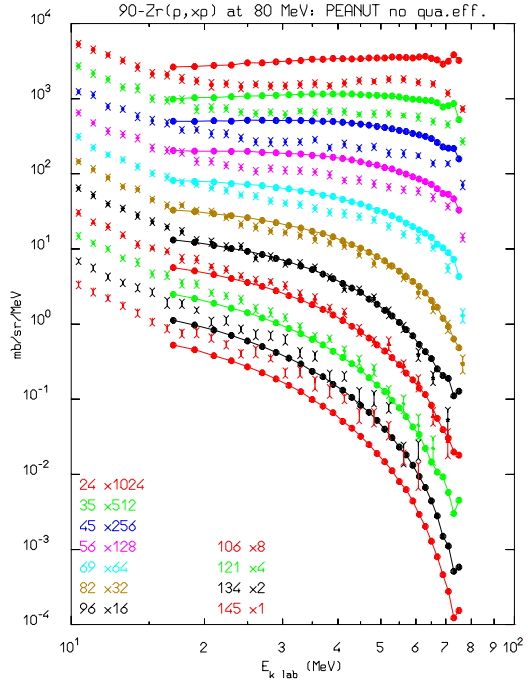

Figure 11: ^{90}Zr(p,xp) at 80.5 MeV, PEANUT (see text) calculation with no quantal effect, but Pauli blocking.

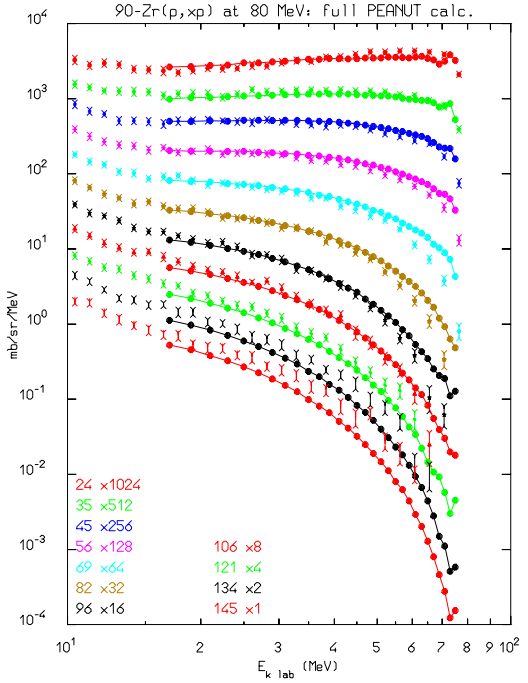

Figure 12: ^{90}Zr(p,xp) at 80.5 MeV, full PEANUT (see text) calculation.

but still there are large discrepancies.

The third trial has been performed switching on all the refraction and reflection business, but still limiting the quantal effects to Pauli blocking alone. There is a great improvement, with still discrepancies at the forward angles, but a reasonable description of backward ones. The reason for these latter deficiencies is related to the effect of particle curvature in the nucleus which both increases the particle track length and hence the reinteraction probability, and at the same time "pushes" particles towards the nucleus centre, again increasing the interaction probability.

The fourth and last trial has been performed with all quantal effects on, that is with coherence length, nucleon correlation, and fermion antisymmetrization effects on. Clearly these are effective in increasing particle mean free paths in the nuclear medium resulting in a quite reasonable

description of the whole spectrum at all angles (see also [22] for the effect of nucleon correlations).

The effect of particle curvature on interaction rates are typical of INC codes which include refraction and reflection [23]. The reason for the good results, at least for angle integrated spectra, of INC models based on straight trajectories (like the Bertini INC) probably lies in the compensating effect of the lack of mechanisms able to lengthen particle mean free paths, and of the curvature effect which operates in the opposite direction. The price is the poor description of angular distributions, at least for energies not much larger than typical potential energies. Such a picture is consistent with what has already been reported in the literature [24, 25, 26, 27].

Of course, many more improvements to the intermediate energy model can be made, and more physical processes should be included. Some work has already been performed with respect to the last published results [7].

3.1 Nuclear densities

What is normally measured in scattering experiments is the nuclear charge density, that means the proton density. The width and shape of its distribution are well known and easily parametrizable. The most straightforward assumption for the *neutron* density is that its shape and width are the same as the proton one. There are however many hints that the neutron density distribution extends to larger radii, creating a neutron halo. Separated density distributions for protons and neutrons have been recently included in PEANUT. Both densities are presently described with symmetrized Woods-Saxon shapes [28], but with different parameters for protons and neutrons. Parameters have been chosen according to the Myers and Swiatecki droplet model [29].

Light nuclei The standard functional representation of the nuclear density is not suitable for very light nuclei, where the skin depth becomes comparable to the core radius. On the other hand, for small nucleon numbers a calculation of the density starting from nucleon wave functions is feasible: solutions using shell model wave functions with a harmonic oscillator potential can be derived analytically, and show good agreement with experimental distributions [30]. The density distributions for N_s nucleons (protons or neutrons) in the s-shell and N_p nucleons in the p-shell are given by [30]:

$$\rho_s(r) = \frac{N_s}{\pi^{\frac{3}{2}} a_s^3} \, \mathrm{e}^{-\left(\frac{r}{a_s}\right)^2} \tag{6}$$

$$\rho_p(r) = \frac{2N_p}{3\pi^{\frac{3}{2}} a_p^3} \left(\frac{r}{a_p}\right)^2 \mathrm{e}^{-\left(\frac{r}{a_p}\right)^2} \tag{7}$$

where a_s and a_p are the length parameters in the oscillator well. To take into account the finite size of the nucleons, these density functions must be folded with the single nucleon density, usually taken to have a Gaussian form.

These folded shell model densities have been adopted in PEANUT for N and Z$\leq$8 (thus up to ^{16}O).

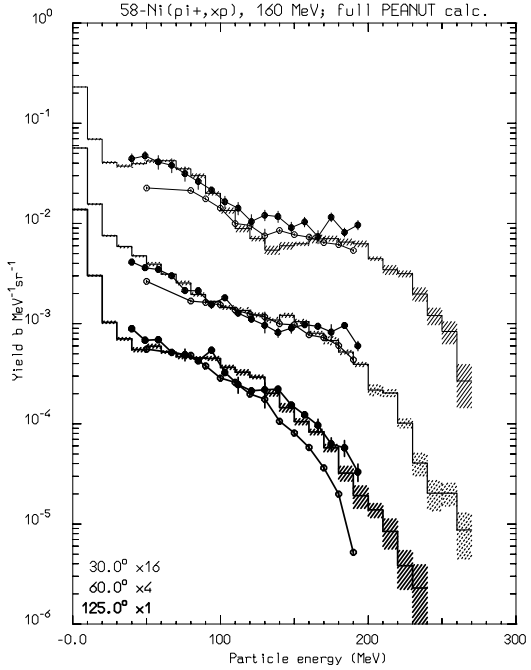

Figure 13: Double differential distribution of protons emitted after π^+ absorption on Ni at 160 MeV pion energy. The experimental data are taken from [31, 32].

3.2 Angular Distribution in Pion Absorption

The differential cross section in the two body pion absorption process is usually written as a Legendre polynomial expansion:

$$\frac{d\sigma}{d\Omega} = \sum_l A_l P_l(\cos(\theta)) \tag{8}$$

Only the terms with $l \leq 4$ are found to be important. Very complete compilations of Legendre coefficients as a function of incident energy exist for pion absorption on a deuteron, or on a pn pair [33, 34]. In this case the odd coefficients vanish, and the A_2 coefficient is of the same size of the A_0 one. The absorption on a pp or pn pair is much less studied, and only a few energy points have been determined [34, 35]. The A_1 term is non-negligible (except for the case of an ingoing π^0) and its sign depends on the projectile charge; the A_2 term is even larger than in pn absorption. It is thus clear that the nucleons outgoing from a two body pion absorption are preferentially forward and backward- emitted. This anisotropy has been included in PEANUT. The values of the A_l coefficients at each energy are computed from fits to available data. This inclusion reflects itself in a better agreement of calculated and experimental results for pion-nucleus absorption, not only for angular distributions but also for emitted nucleons spectra, as shown in fig. 13 (to be compared with the results presented in [7]).

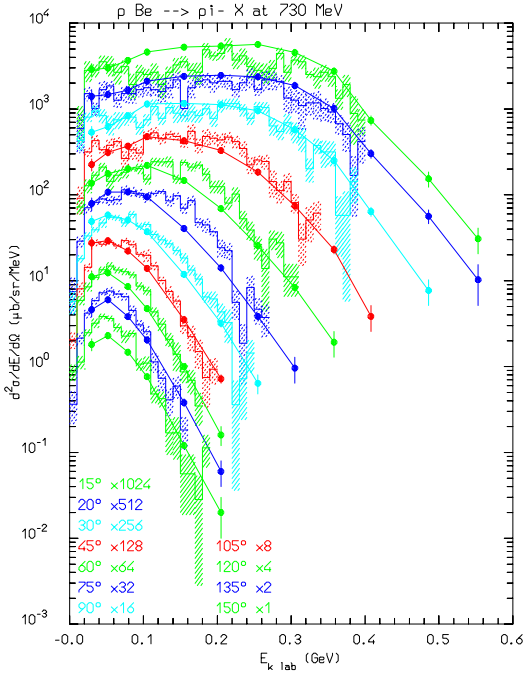

Figure 14: Double differential distribution of negative pions in the reaction p+Be at 730 MeV.

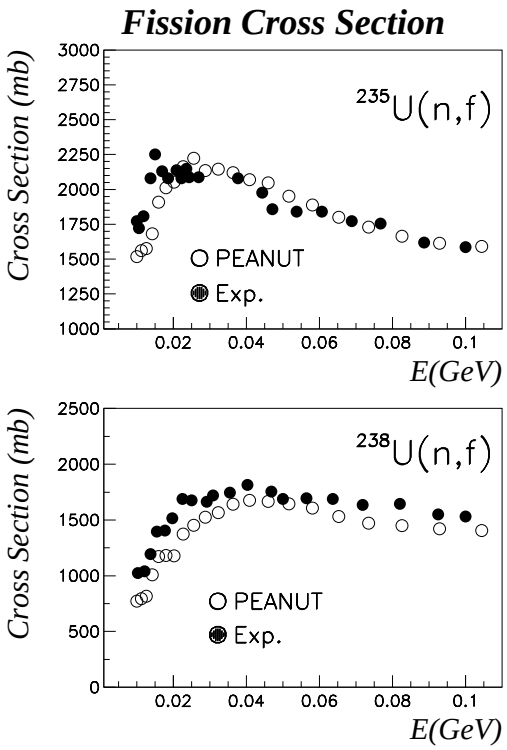

Figure 15: Neutron induced fission cross sections on Uranium. Experimental data are from [43].

3.3 Pion production

Pion production is the first inelastic channel to be open both in pion-nucleon and nucleon-nucleon interactions, obviously because of the small pion mass. The reaction $N_1 + N_2 \rightarrow N_1' + N_2' + \pi$ has its threshold around 290 MeV, and it starts to be important around 700, while the reaction $\pi + N \rightarrow \pi' + \pi'' + N'$ opens at 170 MeV. The dominance of the Δ resonance, and of the N resonances at higher energies, in the π, N channel suggest to treat both reactions in the framework of the isobar model, that is to assume that they all proceed through an intermediate state containing at least one resonance, for instance in the case of the Δ :

(9) $$N_1 + N_2 \rightarrow N_1' + \Delta \rightarrow N_1' + N_2' + \pi$$

and

(10) $$\pi + N \rightarrow \pi' + \Delta \rightarrow \pi' + \pi'' + N'$$

In the intermediate state the resonance can be treated as a real particle, that is, in a Monte Carlo code it can be transported and then transformed into secondaries according to its lifetime and decay branching ratios.

The isobar model accommodates easily multiple pion production, simply allowing the presence of more than one resonance in the intermediate state. These processes are simulated in PEANUT by coupling the resonance production part of the HADRIN [36] code, suitably modified, to all the subsequent intranuclear steps. The relative resonance decay branching ratio in different pion and nucleon charge states have been computed through isospin relations. The results are fairly encouraging, as shown in fig. 14.

3.4 Fission

At the end of the intranuclear cascade the residual nucleus is supposed to be left in an equilibrium state, in which the excitation energy is shared by a large number of nucleons. This energy is further dissipated by several competing mechanisms, with emission of light or heavy fragments and/or photons. The dominant process is evaporation [7, 37, 38], normally followed by γ deexcitation, but for heavy nuclei the fission process cannot be neglected. The model used in PEANUT for fission is the statistical one [37, 39], in the formulation of Atchison [9, 40] (see [41, 42] for details), with some modifications. In particular, we were able to omit the unphysical reduction factor that was applied to the fission width in the original Atchison work [9]. This excitation-dependent factor was introduced in HETC to cut off the fission process at high excitation energies and bring the calculations in agreement with measured data. Our explanation is that a intranuclear cascade model without preequilibrium emission leads to an average overestimation of the nuclear excitation energy at the equilibrium stage. This is not the case for PEANUT, and the agreement with experiment is nice without any arbitrary factor, as shown in fig. 15 for Uranium.

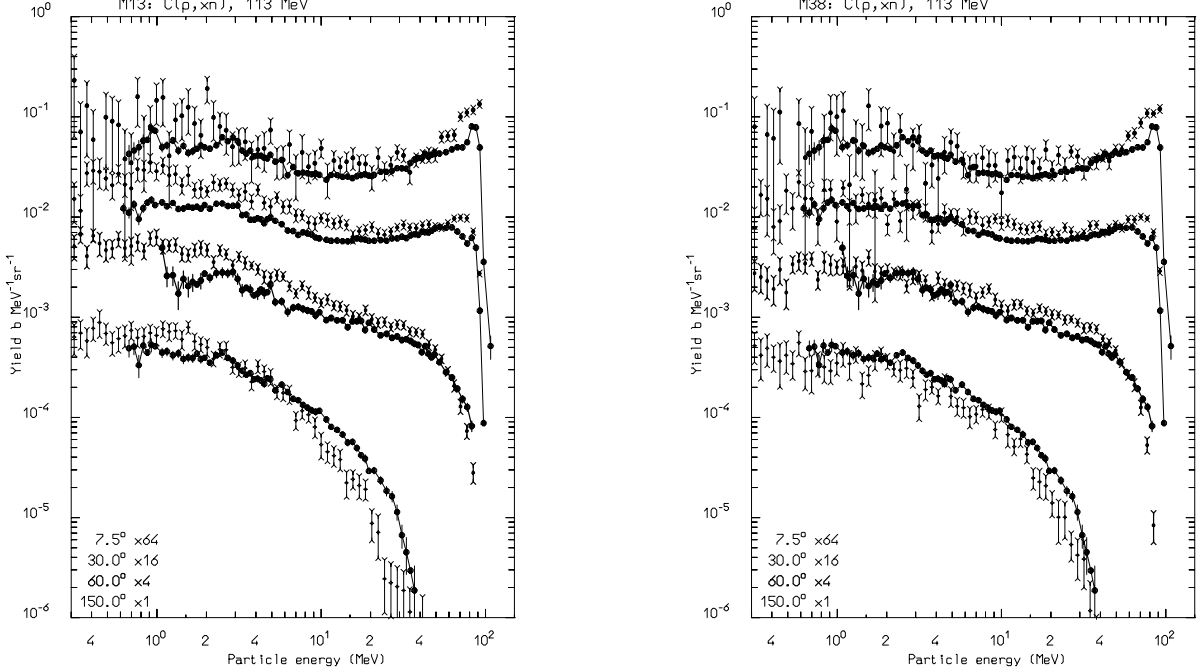

Figure 16: C(p,xn) at 113 MeV, without (left) and with (right) Fermi Break-up in the calculations. Experimental data are from [26].

3.5 Fermi Break-up

For light nuclei, the statistical assumptions and the sequential emission scheme underlying the classical evaporation models become less and less sound, and other deexcitation mechanisms are more suitable for these light (typically A$\leq$16) residual nuclei. The one adopted for FLUKA is the so called Fermi Break-up model [44, 45], where the excited nucleus is supposed to disassemble in just one step into two or more fragments, with branching given by plain phase space considerations. The formulation and the coding adopted in FLUKA are the same as those described elsewhere in this conference [41], thus they are omitted here. The inclusion of Fermi Break-up has eliminated the excess of low-energy evaporation neutrons that was present in former calculations on light nuclei, as shown in fig. 16 for Carbon. It has also greatly improved the residual nuclei distributions, as will be discussed later.

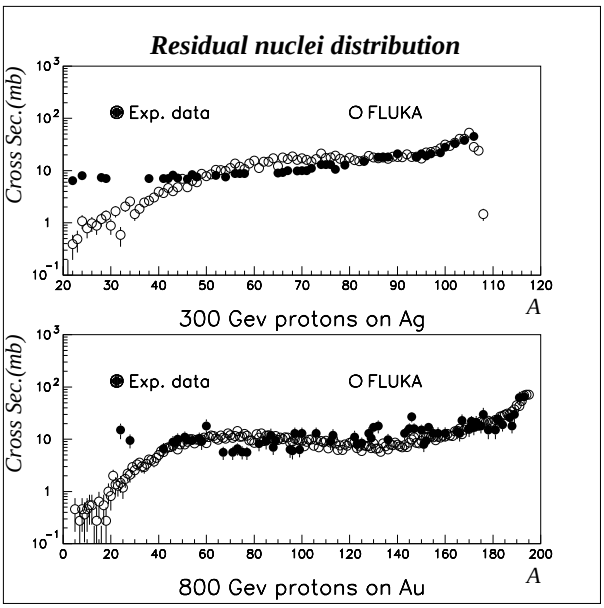

Figure 17: Residual nuclei mass distribution. Experimental data are from [46] for Ag and [47] for gold.

3.6 Residual Nuclei

The problem of a reliable description of individual isotopes produced in hadron-nucleus reactions is still an open one. While the general features of the residual nuclei distributions are usually well reproduced by FLUKA, predictions on individual isotopes can be off by large factors. Many reasons contribute to this uncertainty:

- Slight inaccuracies in excitation energy spectra reaching the evaporation stage can result in small shifts in particle multiplicities, but in substantial shifts among close isotopes
- The lack of spin and parity dependent (Hauser-Feshbach) calculations in the last stage can also bias the very last steps and hence the final residual nucleus
- Charged particle emission channels of low probability can be badly reproduced because of sub-barrier effects etc.

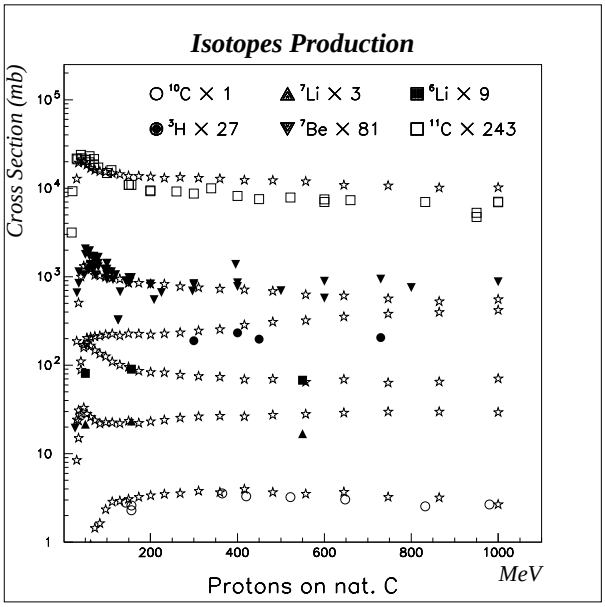

Figure 18: Residual nuclei excitation functions. Experimental data are from [45, 48], open stars are FLUKA results.

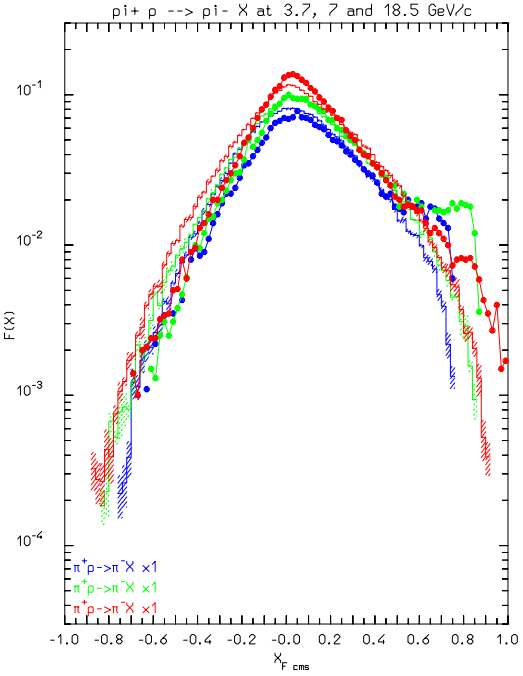

Figure 19: Invariant cross section spectra, as a function of Feynman x_F, of negative pions emitted for π^+ on hydrogen target at various momenta (3.7, 7 and 18.5 GeV/c). Experimental data from [49].

- No prediction about metastable states is possible
- The fragmentation of higher mass compound nuclei is not yet included in the model. This process, although its cross section is usually small, is important when considering the distribution of residual nuclei, because it can produce isotopes very far both from the target mass and from the fission fragment distribution.

Besides these physical reasons, there are also "technical" ones. What is often required when looking for residual nuclei production, is the production cross section of some specific isotopes, for example because of their toxicity or long life time etc., which however can be a very small fraction of the total reaction cross section. Therefore a good agreement over the gross part of emission spectra is not at all a guarantee of a similar agreement on some specific and relatively unlikely isotope production channel. All these remarks apply to other INC codes as well.

Nevertheless, as already said, the overall features of the residual nuclei distribution are well reproduced. In fig. 17 two examples of mass distributions following proton bombardment of heavy nuclei are shown. The calculated distributions are in good agreement with the experimental ones, both in the near-target zone and in the fission product range. There is a clear discrepancy in the low-mass region, due to the lack of fragmentation in the calculations.

Regarding light nuclei, the inclusion of Fermi Break–up has brought about a major improvement in the results on residual nuclei. In fig. 18 the excitation functions for the production of different isotopes by proton bombardment of Carbon are shown. The evaporation model alone could never have explained the abundance of isotopes like ^{7}Be,

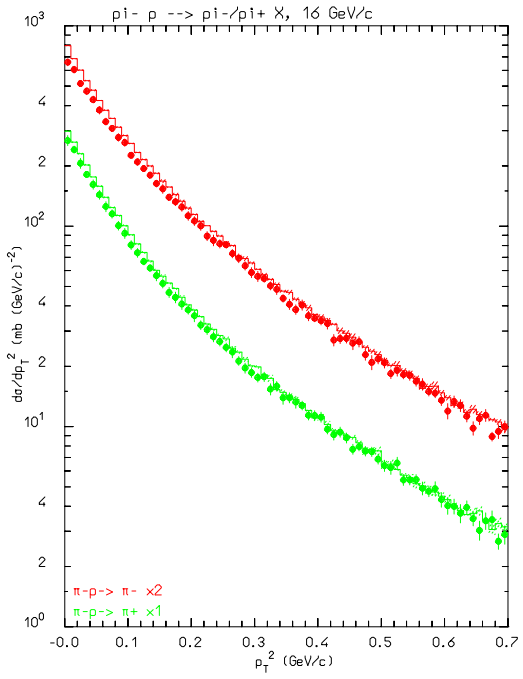

Figure 20: p_T spectra of π^+ and π^- produced by 16 GeV/c π^- incident on a hydrogen target. Experimental data from [49].

while it would have grossly overestimated the emission of neutrons (fig. 16) and α particles (also via the disintegration

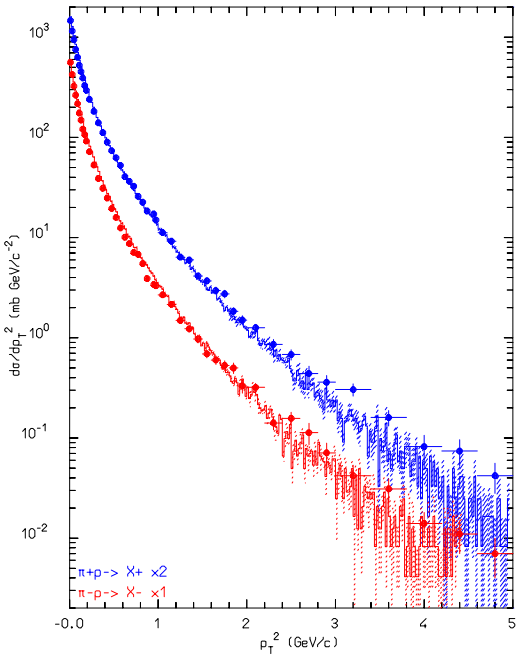

Figure 21: Positive and negative particle p_T distribution for 200 GeV π^+ on hydrogen. Experimental data from [50].

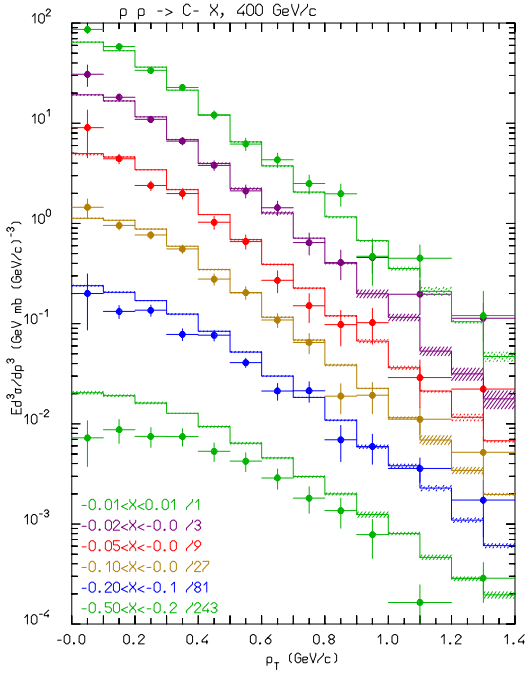

Figure 23: $E\frac{d^3\sigma}{dp^3}$ spectra of negative particles produced by 400 GeV/c protons on a hydrogen target, as a function of p_T and Feynman x in the backward emisphere. Experimental data from [51].

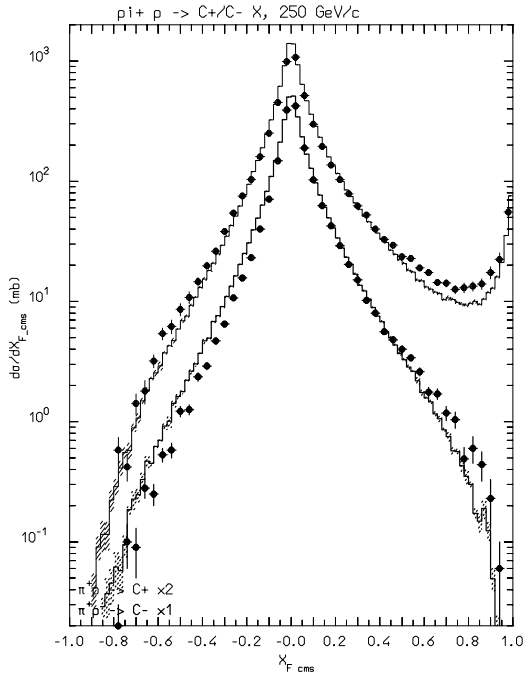

Figure 22: Feynman x_F spectra of positive particles and π^- produced by 250 GeV/c π^+ incident on a hydrogen target. Experimental data from [50].

of ^{8}Be into two α's).

4 HIGH ENERGY HADRONIC INTERACTIONS

Extensive improvements have been carried out in the last years in the model dealing with high energy interactions. The goals of this work were mainly twofold: to obtain agenеral improvement of the high energy event generator also in view of new applications of the code (neutrino beam design, atmospheric neutrino calculations etc.), and to pursue a better description of inelastic interactions in the energy range below 10-20 GeV. The FLUKA high energy event generator is based on the Dual Parton Model (DPM), whose validity is questionable below a few tens of GeV. However, comparisons with experimental data have clearly shown that the resonance model quickly becomes inaccurate for energies above 2–3 GeV, and in particular it is not able at all to predict the correct behaviour of particle x distributions in the central region. This limitation is believed to be a fundamental one, at least for a resonance model with at most two resonances in the starting configuration, and not a lack of sufficiently high mass resonances in the model. Therefore it was felt preferable to stretch in a reasonable way the DPM model towards lower energies, rather than trying to get rid of the problems of the resonance model.

The present DPM based generator is now substantially different and improved with respect to previous FLUKA versions and allows for better predictions both in the central and fragmentation regions. These modifications will not be discussed in detail in this paper because of lack of room and

because the work is still going on. Only a few examples are presented to give a feeling of the present performances, however the topics which underwent major changes are summarized below:

- Introduction of reggeon mediated interactions (single chains) at the lower energy end of the application range of the DPM
- A thorough revision of the chain building process, mainly concerning the use of x fractions and the smooth transition to low energies
- A complete revision of the chain hadronization process with a smooth and physically sound transition to chains made up by only two particles/resonances
- A complete revision of diffractive events which can be now of three different kinds (resonant, single chain and two chain events, the former being related to low mass diffraction and the latter to high mass diffraction)
- Transverse momentum selection and sampling both for chain ends and for individual partons inside the chains
- Use of smeared mass distribution for resonances, according to their experimental width

Some examples of present performances for h–p interactions which are of course the building blocks also for h-A interactions, are shown in figs. 19,20,21,22, 23, both for longitudinal and transverse distributions.

5 CONCLUSIONS

Unlike other codes which have been described at this Workshop, FLUKA cannot count for its development on a full time staff aiming at achieving specified goals in the framework of a well defined project (not to mention budget!). Each upgrade is pursued in general not as a purpose in itself, but under pressure of the need of the moment. As an example, some of the improvements described above were dictated by incursions in fields as diverse as proton therapy (ionization), energy amplifiers (fission), prediction of activation in collider experiments (Fermi break-up).

As the number of attempts to apply the code in new fields increases, new needs arise: but satisfying the latter often opens new possibilities suggesting further applications. It is remarkable how such an anarchical growth has succeeded so far in producing a well balanced and flexible program, in which the equilibrium of the different parts can ensure a similar level of accuracy independent of the type of radiation and application.

6 REFERENCES

[1] A. Ferrari, P. R. Sala, G. Guaraldi and F. Padoani, Nucl. Instr. Meth. B71 (1992) 412.

[2] P. A. Aarnio et al., in " Proc. of the MC93 Int. Conf. on Monte Carlo Simulation in High-Energy and Nuclear Physics", Feb. 22-26, 1993. Ed. P. Dragovitsch, S.L. Linn, M. Burbank, World Scientific, Singapore, 1994, p. 100.

[3] P. A. Aarnio et al., "Proc. of the MC93 Int. Conf. on Monte Carlo Simulation in High-Energy and Nuclear Physics", Feb. 22-26, 1993. Ed. P. Dragovitsch, S.L. Linn, M. Burbank, World Scientific, Singapore, 1994, p. 88.

[4] P. R. Sala and A. Ferrari, "Proc. of the MC93 Int. Conf. on Monte Carlo Simulation in High-Energy and Nuclear Physics", Feb. 22-26, 1993. Ed. P. Dragovitsch, S.L. Linn, M. Burbank, World Scientific, Singapore, 1994, p. 277.

[5] A. Fassò et al, "Proc. of the workshop on Simulating Accelerator Radiation Environment", SARE, Santa Fe, Jan. 11-15, 1993. A. Palounek ed., Los Alamos LA-12835-C 1994, (p. 134).

[6] A. Fassò, A. Ferrari, J. Ranft, and P.R. Sala, " Proc. of the IV Int. Conf. on Calorimetry in High Energy Physics", La Biodola, (Elba), A. Menzione and A. Scribano eds., World Scientific, p. 493 (1994).

[7] A. Fassò, A. Ferrari, J. Ranft, and P. R. Sala, "Proc. of the "Specialists' Meeting on Shielding Aspects of Accelerators, Targets & Irradiation Facilities", Arlington, April 28-29 1994, published by OECD/NEA (1995), 287.

[8] A. Fassò, A. Ferrari and P.R. Sala: "Proc. 8th Int. Conf. Radiation Shielding", Arlington, Texas, April 24-28 1994, American Nuclear Society ed., Vol. 2 (1994), 643.

[9] Intermediate Energy Nuclear Data: Models and codes, Proc. of a specialists' meeting, Issy-les-Moulineaux, May 30th - June 1st 1994, published by OECD/NEA (1994).

[10] G.Z. Molière, Z. Naturforsch. 3a (1948) 78.

[11] G.Z. Molière, Z. Naturforsch. 10a (1955) 177.

[12] B.J. Foote and V.G. Smyth, Nucl. Instr. Meth. B100 (1995) 22.

[13] R.M. Sternheimer, Phys. Rev. 88 (1952) 851; R.M. Sternheimer, S.M. Seltzer, and M.J. Berger, Phys. Rev. B26 (1982) 6067, see also the erratum, B27 (1983) 6971.

[14] H.H. Andersen and J.F. Ziegler, Hydrogen stopping powers and ranges in all elements, Pergamon Press New York 1977, Vol. 3.

[15] Int. Commission on Rad. Units and Measurements, " Stopping Powers and Ranges of Protons and Alpha Particles", ICRU Report 49 (1993)

[16] S.G. Scheib, PhD Thesis, Universität Karlsruhe, 1993.

[17] N. Metropolis et al., Phys. Rev. 100 (1958) 185; N. Metropolis et al., Phys. Rev. 100 (1958) 204.

[18] H.W. Bertini, Phys. Rev. 131 (1963) 1801.

[19] M. Trabandt et al., Phys. Rev. C39 (1989) 452.

[20] A.A. Cowley et al., Phys. Rev. C43 (1991) 678.

[21] *International Code Comparison for Intermediate Energy Nuclear Data*, M. Blann, H. Gruppelaar, P. Nagel and J. Rodens eds., OECD/NEA (1994).

[22] K. Chen et al., Phys. Rev. C4 (1971) 2234.

[23] K. Chen et al., Phys. Rev. 166 (1968) 949; K. Chen et al., Phys. Rev. 176 (1968) 1208.

[24] A. Galonsky et al., Phys. Rev. C14 (1976) 748

[25] F.E. Bertrand, and R.W. Peelle, Phys. Rev. C8 (1973) 1045.

[26] M.M. Meier, D.A. Clark, C.A. Goulding, J.B. McClelland, G.L. Morgan and C.E. Moss, Nucl. Sci. Eng. 102 (1989) 310.

[27] M.M. Meier, W.B. Amian, C.A. Goulding, G.L. Morgan and C.E. Moss, Nucl. Sci. Eng. 110 (1992) 289.

[28] M.E. Grypeos, G.A. Lalazissis, S.E. Massen and C.P. Panos, J. Phys. G 17 (1991) 1093.

[29] W.D. Myers, "Droplet Model of Atomic Nuclei", IFI/Plenum, New York, 1977.

[30] L.R.B. Elton, Nuclear sizes, Oxford University Press, 1961.

[31] W.J. Burger et al., Phys. Rev. C41 (1990) 2215.

[32] R.D. McKeown et al., Phys. Rev. C24 (1981) 211.

[33] D. Ashery and J.P. Schiffer, Ann. Rev. Nucl. Part. Sci. 36 (1986) 207.

[34] H. J. Weyer, Phys. Rep. 195 (1990) 295.

[35] P. Salvisberg et al., Phys. Rev. C46 (1992) 2172.

[36] K. Hänssgen, and J. Ranft, Nucl. Sci. Eng. 88 (1984) 537.

[37] V.F. Weisskopf, Phys. Rev. 52 (1937) 295

[38] I. Dostrowsky, Z. Fraenkel and G. Friedlander, Phys. Rev. 116 (1959) 683.

[39] N. Bohr and J.A. Wheeler, Phys. Rev. 56 (1939) 426

[40] F. Atchison, " Meeting on targets for neutron beam spallation sources", ed. G. Bauer, KFA Jülich Germany, Jül-conf-34 1980.

[41] A. Ferrari, J. Ranft, S. Rösler and P.R. Sala, "Cascade particles, nuclear evaporation and residual nuclei in high-energy hadron-nucleus interactions", this conference.

[42] A. Ferrari, J. Ranft, S. Rösler and P.R. Sala, report ENSLAPP-A-551/95 and submitted to Z. Phys. C.

[43] Lisowski, P.W. et al., "Proc. Int. Conf. on Nuclear Data for Science and Technology", Jülich, Germany, Springer Berlin, 1992 pag. 732.

[44] E. Fermi, Prog. Theor. Phys. 5 (1950) 1570.

[45] M. Epherre and E. Gradsztajn, J. Physique 18 (1967) 48.

[46] N.Y.T. Porile, G.T. Cole and C.Rudy: Phys Rev. C19 (1979) 2288.

[47] L.Sihver et al., Nucl. Phys. A543 (1992) 703.

[48] A.S. Iljinov et al., Landolt-Börnstein, Springer–Verlag, New Series, Vol. 13a (1991)

[49] M.E. Law et al., *A Compilation of Data on Inclusive Reactions*, Internal Report LBL-80 (1972).

[50] M. Adamus, Z. Phys. C39 (1988) 311.

[51] Bromberg et al., Nucl. Phys. B107 (1976) 82.